Supplementary Information

$Ag_2S_2O_8$ meets $AgSO_4$: the second example of metal-ligand valence isomerism among inorganic systems

Tomasz E. Gilewski, Piotr J. Leszczyński, Armand Budzianowski, Zoran Mazej, Adam Grzelak, Tomasz Jaroń, and Wojciech Grochala*

Contents

- O -

S1. Reagents and synthetic procedures; combustion analysis.

I. Reactions were carried out in small FEP Teflon® test tubes using commercially available AgCl and AgF from Sigma-Aldrich. 100% persulfuric acid was obtained in a reaction of distilled chlorosulfonic acid and 100% H_2O_2 obtained from concentrated aqueous solution via distillation (100% H_2O_2 was kindly made available to us by Dr Grzegorz Rarata from the Institute of Aviation in Warsaw; it must be handled in very clean containers (free from transition metal impurities) to avoid its vigorous catalytic decomposition.

$$2HSO_3Cl + H_2O_2 \rightarrow H_2S_2O_8 + 2HCl \qquad (1)$$

Reaction 1 was performed by distilling a 5% excess chlorosulfonic acid onto H_2O_2 in liquid nitrogen temperature, under vacuum. The reaction took place when the mixture was heated to about –20°C. Hydrogen chloride and excess chlorosulfonic acid were subsequently removed with vacuum. The product was a white solid that usually decomposes if kept for a few days at a room temperature.

Powder XRD measurement of solid $H_2S_2O_8$ confirmed that no H_2SO_5 or $H_2S_2O_7$ were present in the sample, which enabled structure solution (section S3).

II. Reactions (2) were performed in small FEP reactors. We used freshly prepared 100% $H_2S_2O_8$. AgF and AgCl (99.99%) were supplied by Sigma-Aldrich.

$$\mathbf{2AgX + H_2S_2O_8 \rightarrow Ag_2S_2O_8 + 2HX \uparrow (X=F, Cl)} \qquad \mathbf{(2)}$$

Reaction (2) using AgF led to explosion, however shortly before it happened we observed creation of a dark brown or black product, which suggests temporary formation of a compound of silver (II) or silver (III). On the other hand, mixture using AgCl did not show any signs of reactivity.

III. $AgSO_3F$, $AgSO_3CF_3$ and $K_2S_2O_8$ were supplied by Sigma-Aldrich, $AgSbF_6$ was prepared according to the published procedure, solvents were obtained from Fluorochem. For preparation procedure of tetra-n-butylamonium persulfate see below. All metathetic reactions (3) were performed at room temperature and in argon atmosphere.

$$\mathbf{2AgX + M_2S_2O_8 \rightarrow Ag_2S_2O_8 + 2MX \qquad X=SbF_6, F, SO_3F, SO_3CF_3, M=K, (n\text{-}C_4H_9)_4N} \qquad \mathbf{(3)}$$

Metathetic reaction using $AgSbF_6$ and $K_2S_2O_8$ was performed in liquid anhydrous HF solvent, using monel vacuum lines and FEP reactors. The solid product of this reaction was a mixture of $Ag_2S_2O_7$ and Ag_2SO_4.

Metathetic reaction using AgF and $[(n\text{-}C_4H_9)_4N]_2S_2O_8$ was conducted in a mixture of (1,1,1,3,3,3)-hexafluoro-propane-2-ol and perfluoro-t-butanol. No reactivity as observed.

Metathetic reaction using $AgSO_3F$ and $[(n\text{-}C_4H_9)_4N]_2S_2O_8$ was conducted in *t*-C_4F_9-OH (in which both reagents poorely dissolve) using magnetic stirrer. The only crystalline product of reaction was Ag_2SO_4; unreacted $AgSO_3F$ was also present.

IV. Tetra-n-butylamonium persulfate was synthesised by metathesis from sodium persulfate and tetra-n-butylammonium hydrogen sulfate, as described previously [Ref.14 in main paper], starting from commercially available Sigma-Aldrich precursors. Extraction of an aqueous solution of sodium peroxydisulfate (with 5% excess) and two equivalents of tetrabutylammonium hydrogen sulfate with methylene chloride, drying, filtration, and evaporation gave white crystals of n-tetrabutylammonium peroxydisulfate and then dried at 25 ^{o}C under high vacuum for a couple days. Combustion analysis confirmed the chemical identity of the product. Compound was dissolved in anhydrous CH_2Cl_2 for subsequent reaction.

Silver tetrakis(perfluoro-t-butoxy)aluminate was purchased from Iolitec, Germany. Powder XRD confirmed that each batch of this compound was virtually identical to others. Silver nanoclusters constitute hardly removable impurity of this compound.

Metathetic reaction (4) was conducted in glass containers at room temperature or at 0 °C; we used CH_2Cl_2 obtained from Sigma-Aldrich, which was first carefully dried over anhydrous $CaSO_4$, as a solvent. Reactions carried out at 0 °C in attempt to minimize the thermal decomposition ofthe product, in fact did not produce better yield than those conducted at room temperature (poor solubility of both precursors in CH_2Cl_2 at 0 °C is one likely reasons or that). We used 5-10% excess of $[(n\text{-}C_4H_9)_4N]_2S_2O_8$ to ensure complete reaction (moreover, small amount of silver tetrakis(perfluoro-t-butoxy)aluminate is present as a solvate with CH_2Cl_2 in the starting reagent, thus ensuring even larger molar excess of $[(n\text{-}C_4H_9)_4N]_2S_2O_8$).

$$\mathbf{2Ag[Al(O\text{-}t\text{-}C_4F_9)_4] + [(n\text{-}C_4H_9)_4N]_2S_2O_8 \rightarrow Ag_2S_2O_8 \downarrow + 2[(n\text{-}C_4H_9)_4N][Al(O\text{-}t\text{-}C_4F_9)_4] \qquad (4)}$$

The product in the solid state is a very fine white powder (slightly beige from nano-Ag impurities) which must be decanted as it passes even through a 1µm mesh filter. It was rinsed 6-10 times with fresh portions of cold anhydrous CH_2Cl_2.

We have conducted reaction (4) six times to make sure that repeatable results are obtained. The chemical identity of the products is always the same ($Ag_2S_2O_8$ > $Ag_2S_2O_7$, Ag_2SO_4), but their relative contents in the sample may differ. In particular, if reaction is repeated at a larger scale the product tends to decompose much faster yielding mostly $Ag_2S_2O_7$ and some Ag_2SO_4.

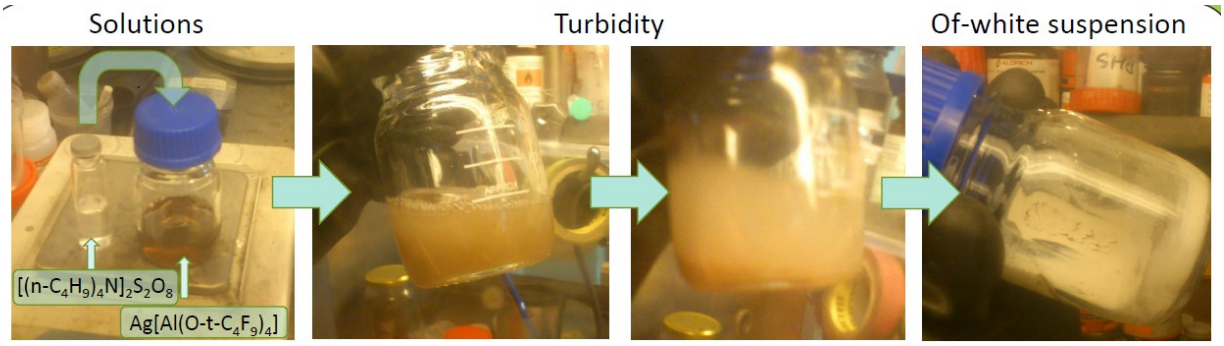

Combustion analysis for S for the typical sample showed 14.64 wt.% S (*vs.* 15.69 wt.% theoretical), which would translate to 93.3% bulk purity, provided that $Ag_2S_2O_8$ is the only S-containing compound. However, since some $Ag_2S_2O_7$ and Ag_2SO_4 are also present, the true $Ag_2S_2O_8$ content is smaller than this value. The sample with the largest contents of $Ag_2S_2O_8$ has been selected for both TGA-DSC-EGA and magnetic VSM-SQUID measurements. However, for structure refinement we have selected a sample which contained only 48.0 wt.% $Ag_2S_2O_8$, 22.7 wt.% Ag2SO4 and 30.0 wt.% $Ag_2S_2O_7$, but the reflections were most narrow thus testifying the best crystallinity.

Metathesis successfully delivers the desired product due to two factors: (i) $Ag_2S_2O_8$ is the least soluble in CH_2Cl_2 among all compounds which could be formed from Ag^+, $[N(n\text{-}Bu)_4]^+$, $[Al(O\text{-}t\text{-}C_4F_9)_4]^-$ and $S_2O_8^{2-}$ ions, and (ii) the larger lattice energy of the product seems to be the driving force, given the difference of ionic sizes for Ag^+ and $S_2O_8^{2-}$ (smaller ions) *vs.* $[N(n\text{-}Bu)_4]^+$ and $[Al(O\text{-}t\text{-}C_4F_9)_4]^-$ (larger ions). The HSAB principle does not necessarily apply, since $[Al(O\text{-}t\text{-}C_4F_9)_4]^-$ seems to be harder anion than $S_2O_8^{2-}$.

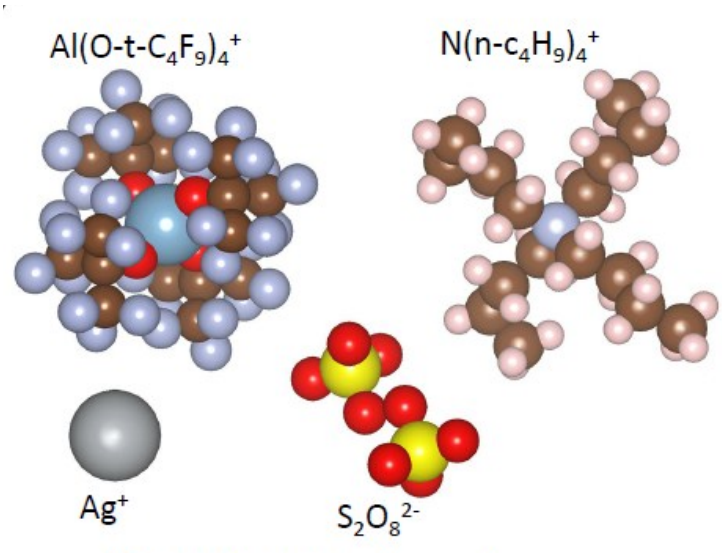

S2. The crystal structure of $Ag_2S_2O_8$ from the Rietveld refinement.

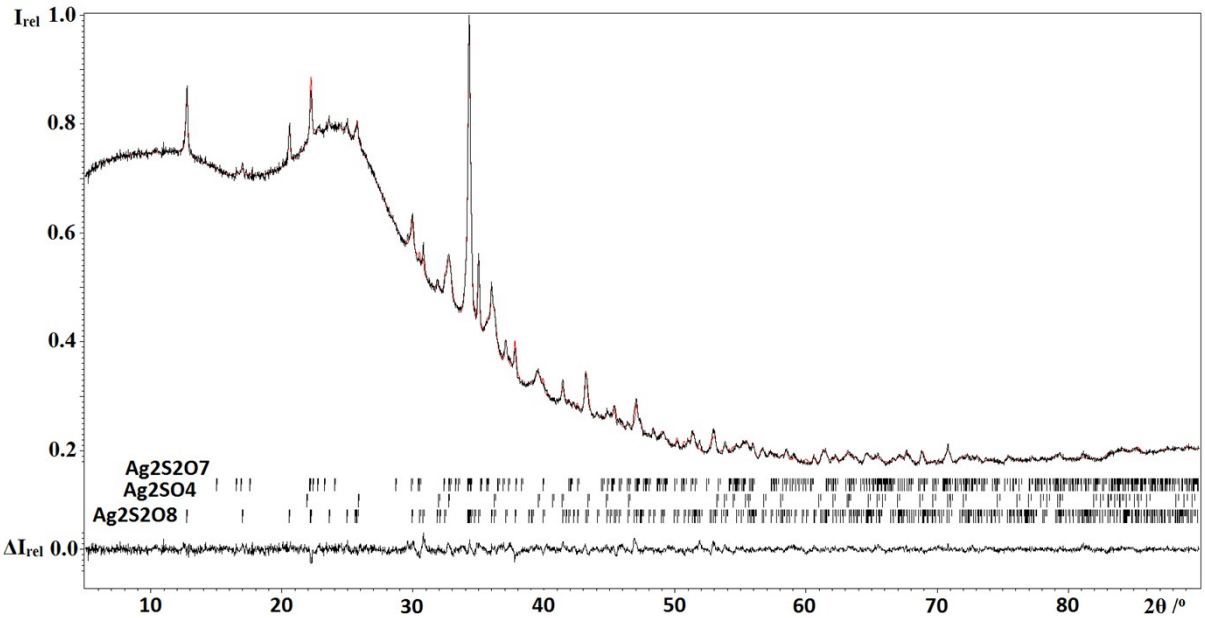


```
-----------------------------------------------------------------------
|R factors for Ag2S2O8 : [532=528+4/75]                                |
|R(obs)=  4.95   wR(obs)=  5.34   R(all)=   5.02   wR(all)=  5.35      |
|R factors for Ag2SO4 : [53=53+0/9]                                    |
|R(obs)=  2.27   wR(obs)=  2.77   R(all)=   2.27   wR(all)=  2.77      |
|R factors for Ag2S2O7 : [302=299+3/9]                                 |
|R(obs)=  2.95   wR(obs)=  3.26   R(all)=   3.15   wR(all)=  3.26      |
|=========================================================================|
|Profile R factors :[3237/60+87],   Damping factor:  0.2000            |
|GOF  =  1.47 Rp   =  0.86 wRp   =  1.17                               |
|Last wRp:  1.17                                                       |
|Maximum change/s.u. :   -0.0422 for z[O3]                             |
-----------------------------------------------------------------------
```

Relative phase amounts in mass

Ag2S2O8 0.56(3) Ag2SO4 0.14(2) Ag2S2O7 0.31(2)

CSD-number formula/filename
431830 Ag2 O8 S2
data_I
_symmetry_cell_setting monoclinic
_symmetry_space_group_name_H-M 'C c'
_symmetry_Int_Tables_number 9
*loop_*
_symmetry_equiv_pos_site_id
_symmetry_equiv_pos_as_xyz
1 x,y,z
2 x,-y,1/2+z
3 1/2+x,1/2+y,z
4 1/2+x,1/2-y,1/2+z
_cell_length_a 9.983(3)
_cell_length_b 16.010(5)
_cell_length_c 6.8837(19)
_cell_angle_alpha 90
_cell_angle_beta 111.745(10)
_cell_angle_gamma 90
_cell_volume 1021.92
*loop_*
_atom_site_label
_atom_site_type_symbol
_atom_site_fract_x
_atom_site_fract_y
_atom_site_fract_z
S1 S 0.769(3) 0.404(2) 0.186(5)
O1 O 0.879(4) 0.438(4) 0.118(8)
O2 O 0.652(4) 0.360(2) 0.000(7)
O3 O 0.830(4) 0.346(3) 0.343(6)
O4 O 0.705(5) 0.470(3) 0.263(7)
S3 S 0.587(4) 0.2327(19) -0.184(6)
O9 O 0.706(5) 0.2766(19) 0.000(7)
O10 O 0.623(5) 0.237(3) -0.369(8)
O11 O 0.577(5) 0.147(2) -0.132(9)
O12 O 0.452(5) 0.274(2) -0.225(8)
Ag1 Ag 0.7468(19) 0.3953(15) 0.573(3)
Ag2 Ag 1.0664(19) 0.5063(16) 0.092(3)
Ag3 Ag 0.558(2) 0.2256(14) -0.721(3)
S2 S 0.417(5) 0.417(3) 0.451(9)
S2' S 0.362(5) 0.622(3) 0.720(10)
O5 O 0.334(5) 0.487(4) 0.538(14)
O5' O 0.220(7) 0.597(3) 0.675(16)
O6 O 0.538(4) 0.386(4) 0.619(10)
O6' O 0.436(11) 0.631(6) 0.944(11)
O7 O 0.464(11) 0.455(5) 0.297(12)
O7' O 0.363(5) 0.700(4) 0.620(14)
O8 O 0.319(6) 0.349(5) 0.357(15)
O8' O 0.444(5) 0.553(4) 0.633(14)
O4 O 0.705(5) 0.530(3) 0.763(7)
Ag1 Ag 0.7468(19) 0.6047(15) 0.073(3)
Ag2 Ag 0.0664(19) 0.4937(16) 0.592(3)

Ag3 Ag 0.558(2) 0.7744(14) 0.779(3)
S2 S 0.417(5) 0.583(3) 0.951(9)
S2' S 0.362(5) 0.378(3) -0.780(10)
S2' S 0.362(5) 0.378(3) 0.220(10)
O5' O 0.220(7) 0.403(3) 0.175(16)
O5' O 1.220(7) 0.403(3) 0.175(16)
O6 O 0.538(4) 0.614(4) 1.119(10)
O6' O 0.436(11) 0.369(6) 0.444(11)
O7 O 0.464(11) 0.545(5) 0.797(12)
O7' O 0.363(5) 0.300(4) -0.880(14)
O8 O 0.319(6) 0.651(5) 0.857(15)
O8' O 0.444(5) 0.447(4) 0.133(14)

#END

Constraints applied

```
loop_
 _restr_distance_atom_site_label_1
 _restr_distance_site_symmetry_1
 _restr_distance_atom_site_label_2
 _restr_distance_site_symmetry_2
 _restr_distance_target
 _restr_distance_target_weight_param
S1 . O1 . 1.45 0.02
S1 . O3 . 1.45 0.02
S1 . O4 . 1.45 0.02
S3 . O11 . 1.45 0.02
S3 . O12 . 1.45 0.02
S3 . O10 . 1.45 0.02
S2 . O6 . 1.45 0.02
S2 . O7 . 1.45 0.02
S2 . O5 . 1.6 0.02
S2 . O8 . 1.6 0.02
S1 . O2 . 1.64 0.02
S3 . O9 . 1.64 0.02
O2 . O9 . 1.48 0.02
O5 . O8 2_565 1.48 0.02
O1 . S3 4_555 2.5 0.08
O7 . O11 4_455 2.5 0.1
O1 . O12 4_555 2.2 0.08
O1 . O11 4_555 2.2 0.08

loop_
 _restr_angle_atom_site_label_1
 _restr_angle_site_symmetry_1
 _restr_angle_atom_site_label_2
 _restr_angle_site_symmetry_2
```

```
 _restr_angle_atom_site_label_3
 _restr_angle_site_symmetry_3
 _restr_angle_target
 _restr_angle_target_weight_param
O1 . S1 . O2 . 109.47 0.1
O1 . S1 . O3 . 109.47 0.1
O1 . S1 . O4 . 109.47 0.1
O2 . S1 . O3 . 109.47 0.1
O2 . S1 . O4 . 109.47 0.1
O3 . S1 . O4 . 109.47 0.1
O9 . S3 . O10 . 109.47 0.1
O9 . S3 . O11 . 109.47 0.1
O9 . S3 . O12 . 109.47 0.1
O10 . S3 . O11 . 109.47 0.1
O10 . S3 . O12 . 109.47 0.1
O11 . S3 . O12 . 109.47 0.1
O5 . S2 . O6 . 109.47 0.1
O5 . S2 . O7 . 109.47 0.1
O5 . S2 . O8 . 109.47 0.1
O6 . S2 . O7 . 109.47 0.1
O6 . S2 . O8 . 109.47 0.1
O7 . S2 . O8 . 109.47 0.1
S1 . O2 . O9 . 104.5 0.1
S3 . O9 . O2 . 104.5 0.1
S2 . O5 . O8 2_565 104.5 0.1
S2 2_565 O8 2_565 O5 . 104.5 0.1

loop_
 _restr_torsion_atom_site_label_1
 _restr_torsion_site_symmetry_1
 _restr_torsion_atom_site_label_2
 _restr_torsion_site_symmetry_2
 _restr_torsion_atom_site_label_3
 _restr_torsion_site_symmetry_3
 _restr_torsion_atom_site_label_4
 _restr_torsion_site_symmetry_4
 _restr_torsion_angle_target
 _restr_torsion_weight_param
S1 . O2 . O9 . S3 . 180 0.5
S2 . O5 . O8 2_565 S2 2_565 180 0.5
```

S3. The crystal structure of $H_2S_2O_8$ from the Rietveld refinement.

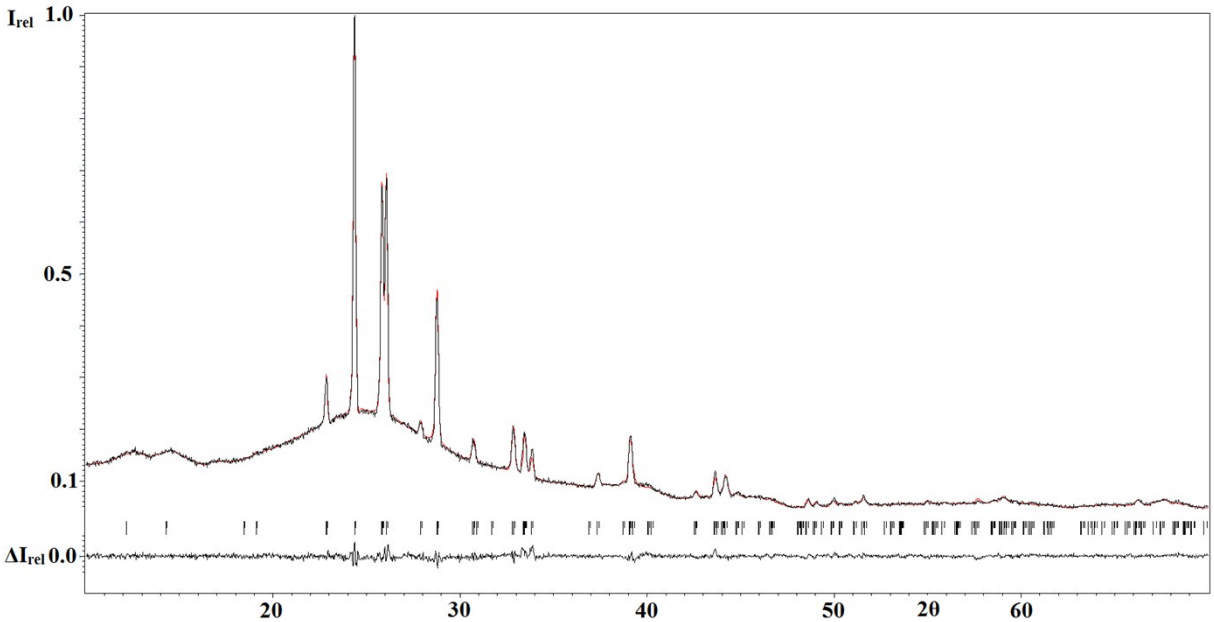


```
-----------------------------------------------------------------------------------------------------------
|R factors : [156=98+58/40]                                                                                |
|R(obs)=   6.34    wR(obs)=   5.77    R(all)=    8.34    wR(all)=   5.97                                |
|=========================================================================================================|
|Profile R factors :[2285/13+40],    Damping factor:   0.1000                                              |
|GOF   =  1.43 Rp    =  2.17 wRp    =  2.90                                                               |
|Last wRp:  2.90  2.90  2.90  2.90  2.90  2.90  2.90  2.90                                                 |
|Maximum change/s.u. :   -0.0486 for z[O6]                                                                 |
-----------------------------------------------------------------------------------------------------------
```

CSD-number formula/filename
430224 H2 O8 S2

```
data_I
_symmetry_cell_setting          triclinic
_symmetry_space_group_name_H-M   'P -1'
_symmetry_Int_Tables_number      2
loop_
_symmetry_equiv_pos_site_id
_symmetry_equiv_pos_as_xyz
1 x,y,z
2 -x,-y,-z
_cell_length_a                  4.7651(14)
_cell_length_b                  7.603(2)
_cell_length_c                  8.503(3)
_cell_angle_alpha               91.894(14)
_cell_angle_beta                90.03(2)
_cell_angle_gamma               108.17(2)
_cell_volume                    292.516
loop_
_atom_site_label
```

```
_atom_site_type_symbol
_atom_site_fract_x
_atom_site_fract_y
_atom_site_fract_z
S1 S -0.542(5) 0.258(3) 0.7294(17)
O1 O -0.735(5) 0.101(4) 0.834(3)
O2 O -0.721(8) 0.295(5) 0.591(4)
O3 O -0.418(9) 0.439(4) 0.822(3)
O4 O -0.277(8) 0.209(5) 0.659(4)
S2 S -0.787(5) -0.228(3) 0.7766(15)
O5 O -0.463(7) -0.195(5) 0.802(5)
O6 O -0.852(7) -0.052(4) 0.713(4)
O7 O -0.898(12) -0.396(4) 0.662(3)
O8 O -0.941(7) -0.287(6) 0.938(4)
H2 H -0.83(2) -0.35(2) 0.984(8)
H1 H -0.716(15) 0.414(6) 0.607(7)

#END
```

Constraints applied

```
loop_
 _restr_distance_atom_site_label_1
 _restr_distance_site_symmetry_1
 _restr_distance_atom_site_label_2
 _restr_distance_site_symmetry_2
 _restr_distance_target
 _restr_distance_target_weight_param
S1 . O1 . 1.6 0.01
S2 . O6 . 1.6 0.01
H1 . O2 . 0.9 0.001
H2 . O8 . 0.9 0.001
O3 . O8 . 2.65 0.03
O2 . O4 1_455 2.65 0.03
O2 . O7 1_455 2.65 0.03
O1 . O6 1_445 1.48 0.01
O7 . H1 1_655 2 0.02

loop_
 _restr_angle_atom_site_label_1
 _restr_angle_site_symmetry_1
 _restr_angle_atom_site_label_2
 _restr_angle_site_symmetry_2
 _restr_angle_atom_site_label_3
 _restr_angle_site_symmetry_3
 _restr_angle_target
 _restr_angle_target_weight_param
S1 . O2 . H1 . 104.5 0.05
S2 . O8 . H2 . 104.5 0.05
O8 . H2 . O3 2_567 180 5
O2 . H1 . O7 1_455 180 5
```

```
loop_
 _restr_equal_distance_atom_site_label_1
 _restr_equal_distance_site_symmetry_1
 _restr_equal_distance_atom_site_label_2
 _restr_equal_distance_site_symmetry_2
 _restr_equal_distance_class_class_id
 _restr_equal_distance_class_target_weight_param
S1 . O2 . 1 0.01
S1 . O3 . 1 0.01
S1 . O4 . 1 0.01
S2 . O8 . 1 0.01
S2 . O5 . 1 0.01
S2 . O7 . 1 0.01

loop_
 _restr_equal_angle_atom_site_label_1
 _restr_equal_angle_site_symmetry_1
 _restr_equal_angle_atom_site_label_2
 _restr_equal_angle_site_symmetry_2
 _restr_equal_angle_atom_site_label_3
 _restr_equal_angle_site_symmetry_3
 _restr_equal_angle_class_class_id
 _restr_equal_angle_class_target_weight_param
O3 . S1 . O2 . 1 0.1
O3 . S1 . O4 . 1 0.1
O2 . S1 . O4 . 1 0.1
O5 . S2 . O7 . 1 0.1
O5 . S2 . O8 . 1 0.1
O7 . S2 . O8 . 1 0.1
O1 . S1 . O2 . 1 0.1
O1 . S1 . O3 . 1 0.1
O1 . S1 . O4 . 1 0.1
O6 . S2 . O8 . 1 0.1
O6 . S2 . O5 . 1 0.1
O6 . S2 . O7 . 1 0.1
S1 . O1 . O6 1_445 1 1
S2 . O6 . O1 1_665 1 1
```

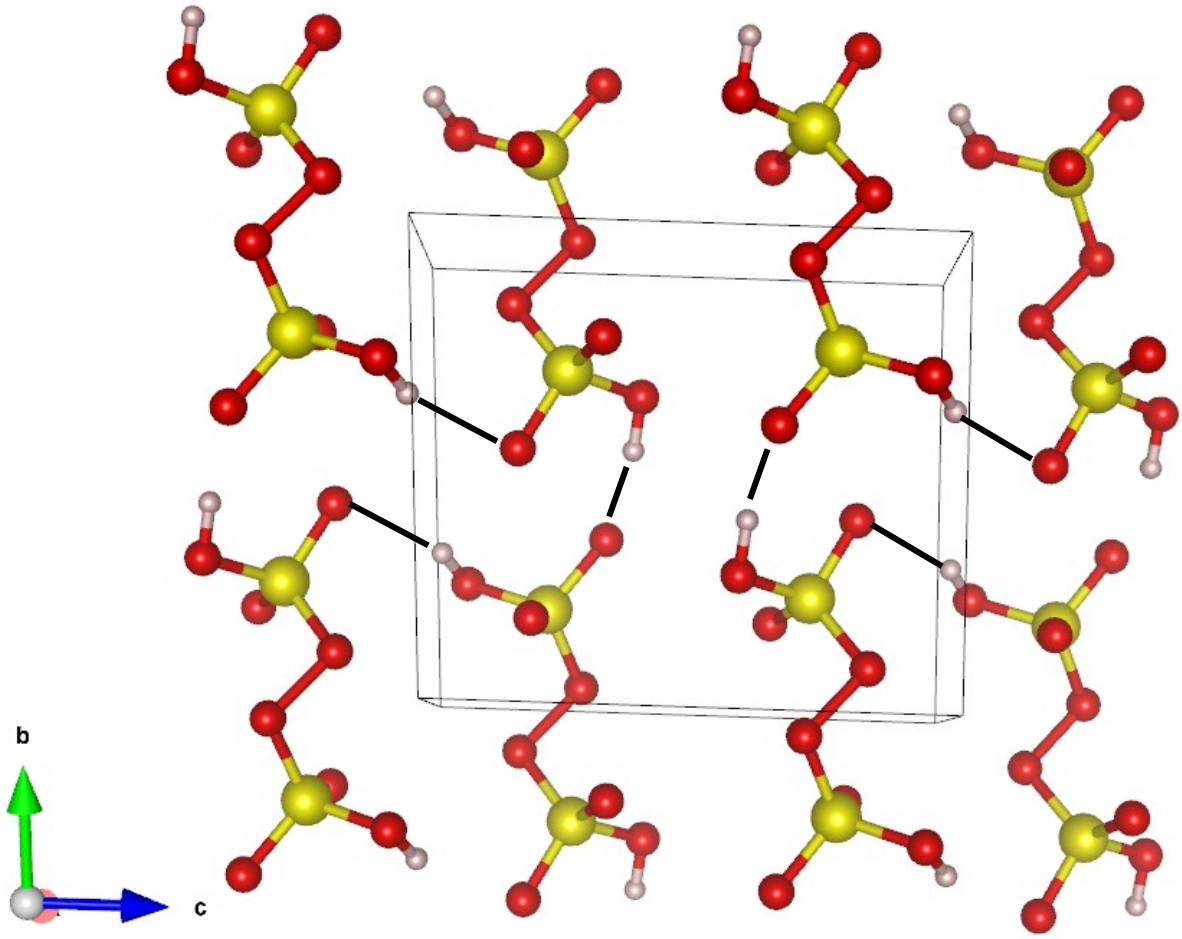

Expanded unit cell of $H_2S_2O_8$; selected weak intermolecular hydrogen bonds are marked with dash black lines.

The triclinic unit cell of $H_2S_2O_8$ contains 2 FUs related by inversion center; moderately strong intermolecular hydrogen bonds at 1.95(6) Å (O…O separation of 2.78(4) Å) along the ***b*** axis bind adjacent molecules in pairs; additional much weaker hydrogen bonds at 2.27(8) Å (O…O separation of 3.13(5) Å) interconnect the so-formed dimers. Obviously, the positions of H atoms cannot be determined precisely from the x-ray powder data. However, the IR and Raman spectra published previously in the literature (Mathias Hopfinger, PhD Thesis, Ludwig-Maximilians-Universität München **2012**) confirms the presence of the moderately strong hydrogen bonds in the crystal structure of $H_2S_2O_8$.

S4. XPS spectrum of $Ag_2S_2O_8$.

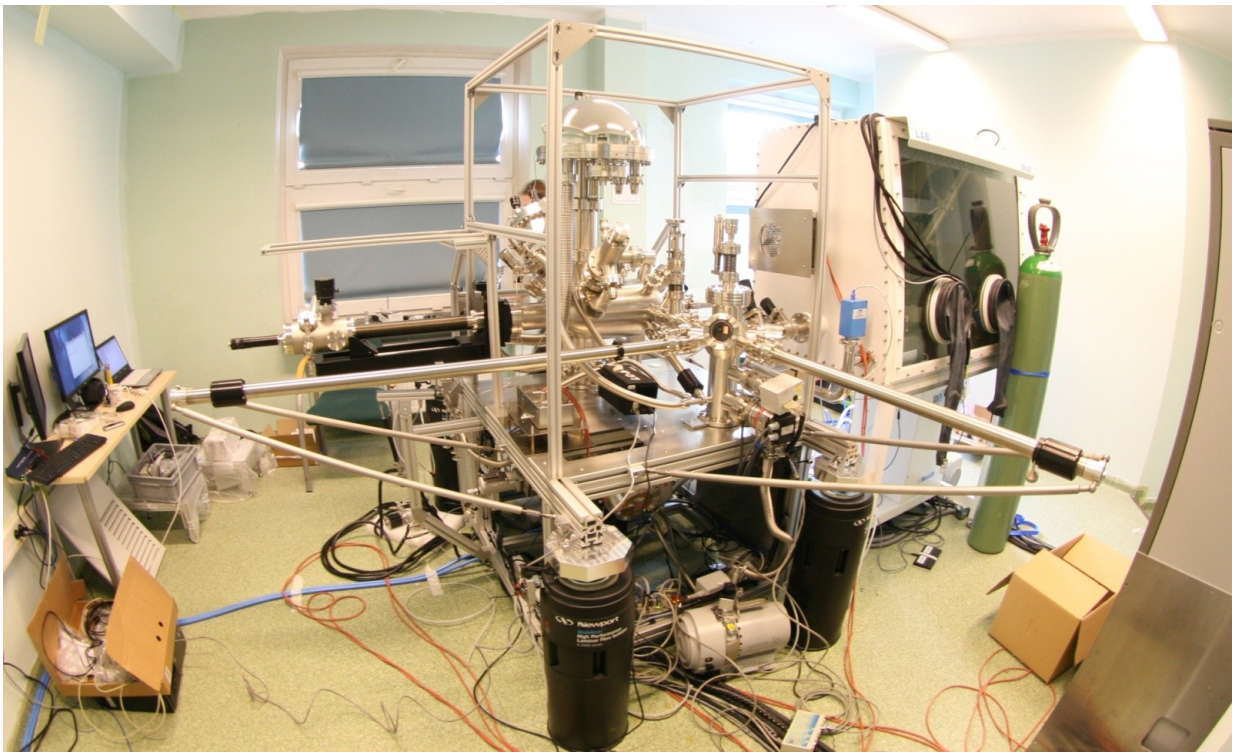

The SPECS system (XPS/UPS/LEED/SEM/Auger) connected to the MBraun glovebox.

The XPS spectrum of $AgSO_4$ has been analyzed in detail in Ref.21 in the main paper (*cf.* also ESI). Other details of our experimental setup and parameters of measurements are also given in that reference. Electron gun was used for charge compensation at electrically insulating surface.

The XPS spectrum of freshly prepared $Ag_2S_2O_8$ (<u>not calibrated = BE as measured</u>) is shown in Figure below. The surface of the compacted sample was refreshed by the knife inside the XPS chamber. Sample placed on the cold finger was permanently cooled with LN2 to *ca.* 100 K to minimize its decomposition in vacuum. The elemental contents was estimated based on Ag(3d), S(2p) and O(1s) intensities. The as measured spectrum is followed by the spectra of the same sample which spent 7 and 12 days in vacuum, and then was heated to 50 ^{o}C and 70 ^{o}C. The initial spectrum is broad and further broadens in time. Two components (of each of the Ag $3d_{5/2}$ & Ag $3d_{3/2}$ bands) are clearly seen after 12 days in vacuum. One of them increases and another diminishes its intensity upon additional heating to 50 ^{o}C and then 70 ^{o}C. Even after prolonged eating to 70 ^{o}C in vacuum, two components are clearly seen. This may correspond to two distinct Ag(I) sites in the high-temperature form of $Ag_2S_2O_8$ and/or in product of its partial decomposition.

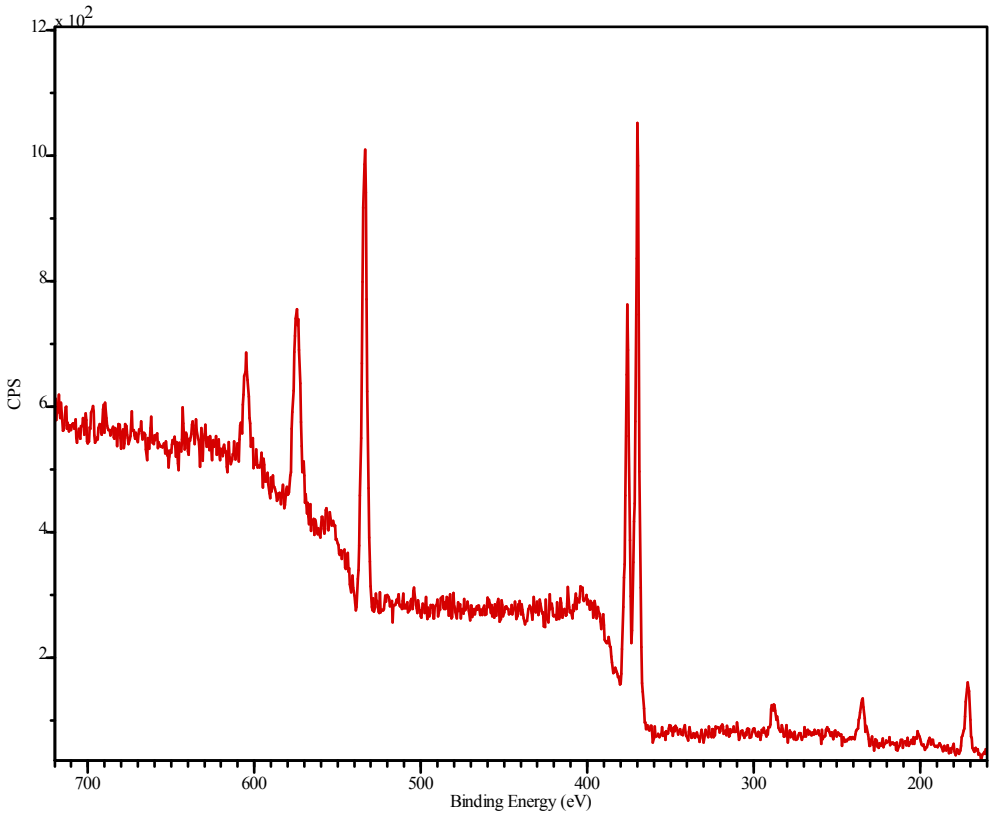

Initial survey spectrum. Composition before heating: **Ag 17.0%, S 15.6%, O 67.4%**.

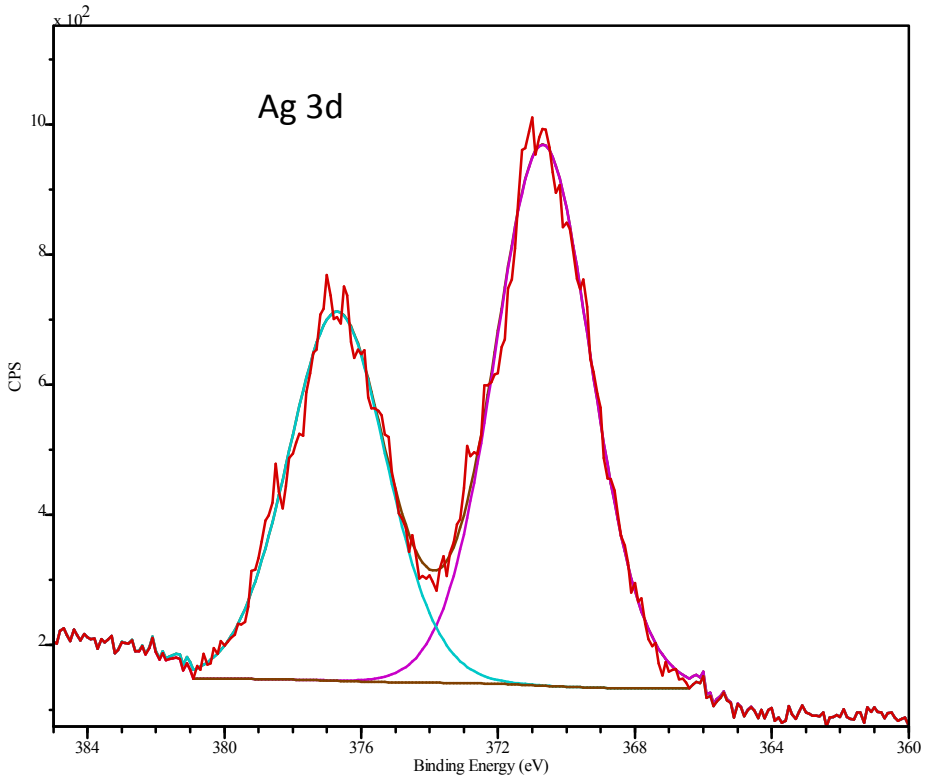

Ag 3d region (fresh sample).

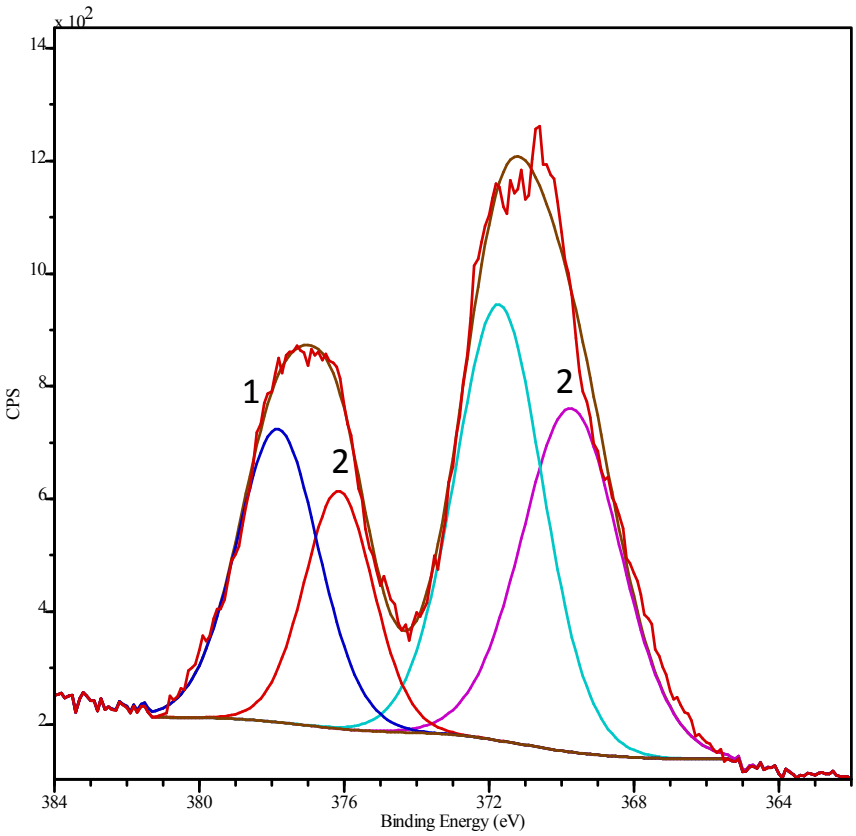

Ag 3d region (after 7 days).

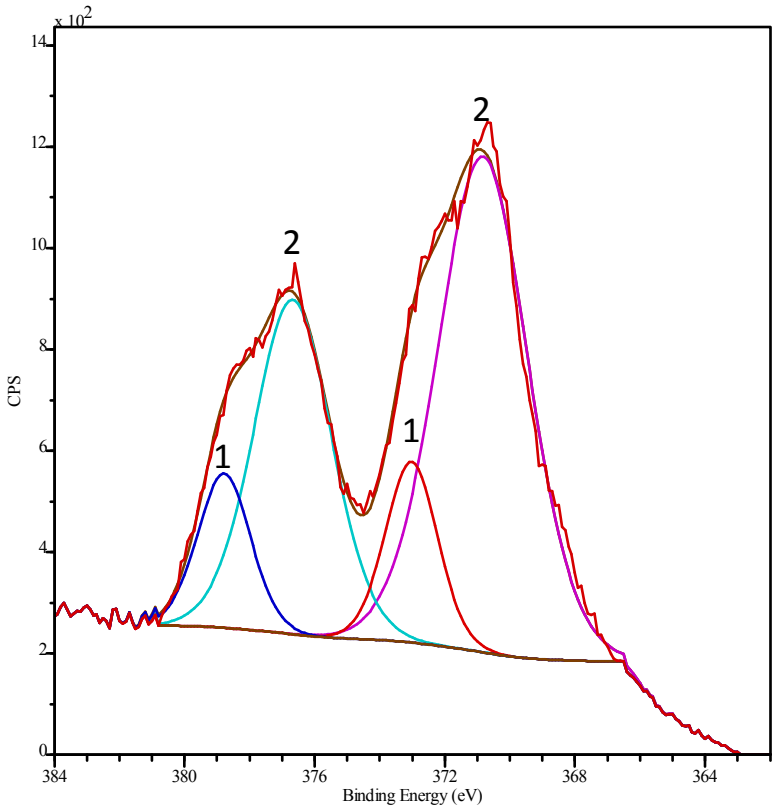

Ag 3d region (after 12 days).

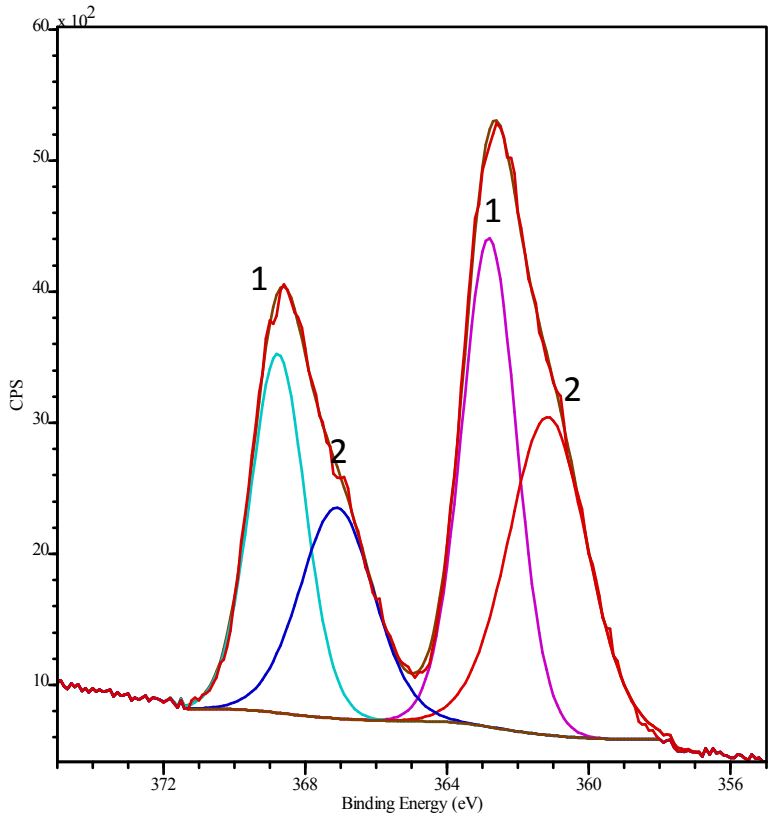

Ag 3d region (after additional heating at 50 °C).

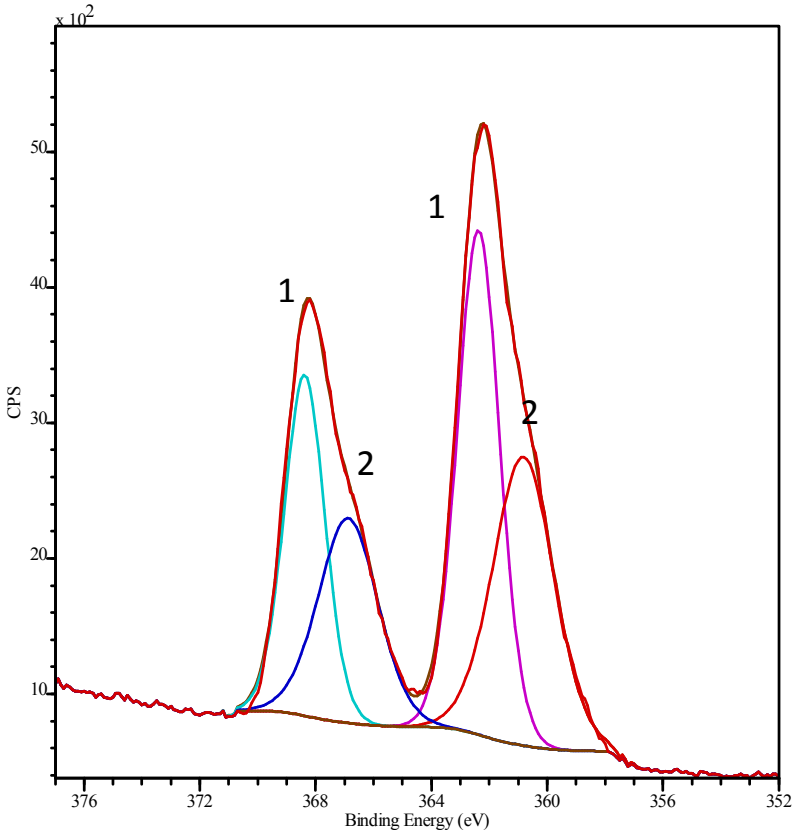

Ag 3d region (after additional heating at 70 °C).

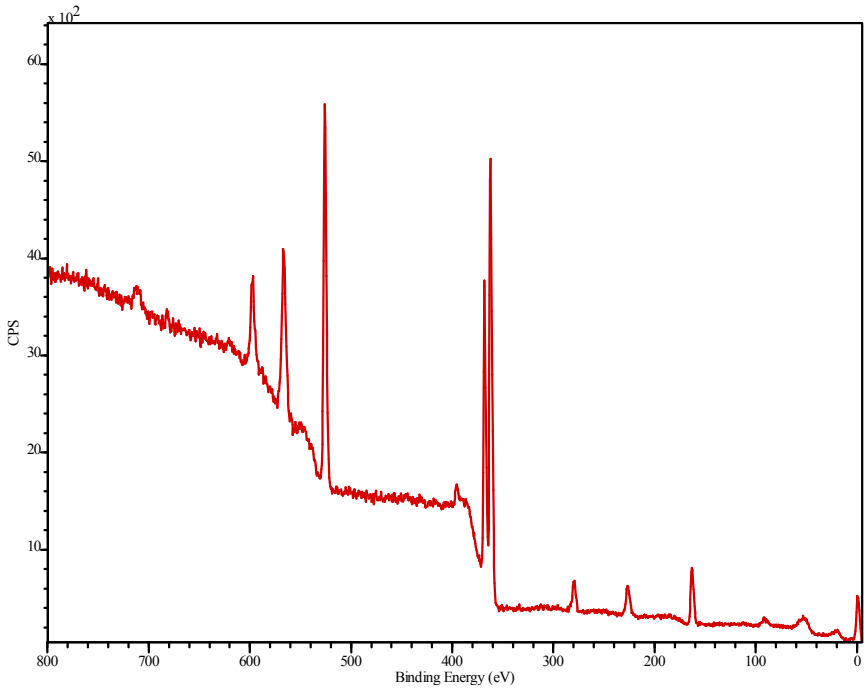

Final survey spectrum. Composition after heating: **Ag 17.9%, S 17.4%, O 64.6%.**

Calibration of the BE values was done by referencing the measured BE to that of the C (1s) signal (the reference value 284.6 eV). Only for some samples a very small F(1s) signal could also be seen, especially after long heating of the sample at 70 °C, which is supposedly due to small contents of the $[Al(O\text{-}t\text{-}C_4F_9)_4]^-$ anion. The small intensity of this signal suggests that occlusion of the Al-containing precursor (or by-product) has not been extensive. However, since F(1s) signal was scarce it could not be consistently used for the referencing procedure. The referenced Ag $3d_{5/2}$ BE value of $Ag_2S_2O_8$ falls at 367.1 eV. One of the referenced values for the product of its decomposition in vacuum is at 365.7 eV (very close to one of the components of the signal previously reported for $Ag_2S_2O_7$), and another at 367.3 eV (thus within error bar of ±0.2 eV from the initial value, and possibly corresponding to the high-temperature phase of $Ag_2S_2O_8$ or even the unreacted substrate).

	Ag $3d_{5/2}$	**Ag $3d_{3/2}$**	**other**
Starting $Ag_2S_2O_8$	367.1	373.1	C 1s: 288.1
Final spectrum (70 °C)	367.3 365.7	373.3 371.8	C 1s: 279.6

The elemental contents (calibrated to total 100% contents of Ag, S & O) estimated from the final spectrum taken after heating at 70 °C is as follows: Ag : S : O = **1 : 0.97 : 3.61** molar %. As compared to the initial ratio of **1 : 0.92 : 3.96**, these values point out to partial elimination of volatile O_2, in fair agreement with TGA-DSC-EGA data (below). Note that the 1 : 1 : 3.5 ratio would correspond to some form of $Ag_2S_2O_7$, or a mixture of this average composition. Note, however, that the behaviour of the sample in high vacuum and during x-ray and electron gun bombardment may be more complex than during thermal decomposition in Ar gas (see below for TGA-DSC-EGA results). Moreover, the surface

layers of the sample probed by x-ray may simply become rich in heavier elements (Ag, S) due to preferential removal of light O atoms.

Table below summarizes the obtained Ag $3d_{5/2}$ & Ag $3d_{3/2}$ BE values for $Ag_2S_2O_8$ together with those for its electromer, $AgSO_4$, and several related compounds (*cf.* ESI to Ref.14 in the main paper).

	Ag $3d_{5/2}$	**Ag $3d_{3/2}$**	**other**	**Ag $3d_{5/2}$ lit.[b]**
$Ag_2S_2O_8$	367.1	373.1	C 1s: 288.1	-
$AgSO_4$*	370.1	376.1	-	-
Ag_2SO_4	368.0	374.0	-	368.0
$AgHSO_4$	368.1	374.1	-	-
$AgSO_3F$*	366.2	372.2	F 1s: 686.8	-
$AgSO_3CF_3$†	368.5	374.5	F 1s: 688.2 C 1s: 292.0	-
$Ag_2S_2O_7$*	369.3 365.9	375.3 371.9	-	-

*Comparison of XPS binding energies of silver compounds studied in this work. All values given in eV and referenced to C 1s line of inadvertent carbon contamination (284.6 eV), except: †F 1s line of $NaSO_3CF_3$ (688.2 eV)[a], *Ag $3d_{5/2}$ line of Ag_2SO_4 internal standard (368.0 eV). "ND" indicates that this particular value was not determined due to rapid decomposition processes and concomitant complexity of this spectral region.*

[a] D. Martin-Vosshage and B. V. R. Chowdari, *J. Electrochem. Soc.*, 1993, **140**, 3531.
[b] V. K. Kaushik, *J. Elec. Spectr. Rel. Phenom.*, 1991, **56**, 273.

S5. Magnetic properties of a sample of $Ag_2S_2O_8$.

Magnetic susceptibility for the 5.2 mg sample of $Ag_2S_2O_8$ was measured in the 1.8–300 K temperaturę range using VSM-SQUID from Quantum Design. Molar susceptibility was calculated while approximating the molar contents of this phase to 100%,and subtracting the contribution from the core electrons. Both the zero-field-cooled and field-cooled measurements were performed in the field of 1000 Oe.

Aside from a „bump" at *ca.* 40 K, which is typical of solid O_2 (recall: samples of $Ag_2S_2O_8$ slowly decompose at room temperature while evolving $Ag_2S_2O_7$ and O_2) and a small Curie tail at temperature below 10 K (which is assigned to a tiny fraction of ferromagnetic impurities) the sample shows diamagnetic response.

In only one sample we have observed a very small maximum at *ca.* 285 K (which is characteristic of Ag(II)SO_4; *cf.* Ref.10 in the main paper) overlapped with diamagnetic signal. It is uncertain if very small amount of $AgSO_4$ was formed during synthesis of $Ag_2S_2O_8$ or rather originated from sponatenous transformation:

$Ag(I)_2S_2O_8 \rightarrow 2\ Ag(II)SO_4$ (5)

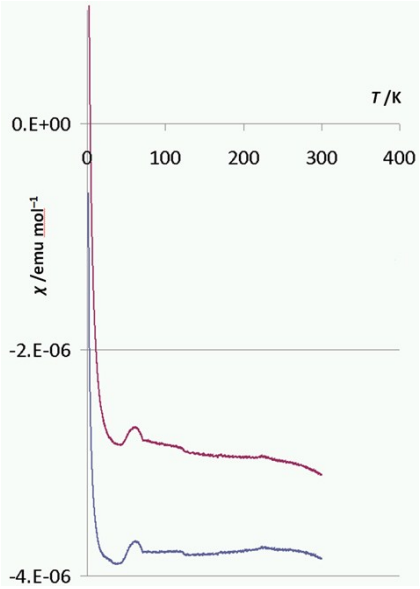

The plot of molar magnetic susceptibility vs. temperature for a typical sample of $Ag_2S_2O_8$ (field-cooled – top, and zero-field-cooled – bottom).

S6. Evolution of the IR spectrum of $Ag_2S_2O_8$ upon heating to 50 °C for 1/3 hr.

The IR spectrum of the sample of $Ag_2S_2O_8$ heated to 50 °C for 20 min, and cooled down to room temperature, is compared to the original spectrum in the figure below (upper spectrum is upshifted in vertical scale for clarity). The relative decay of the bands in the 800-900 cm^{-1} region (corresponding to O-O stretch of the $S_2O_8^{2-}$ anion, **) is seen together with some other spectral changes (especially in the 650-750 cm^{-1}, coming from the S-O-S stretch of the $S_2O_7^{2-}$ anion, *).

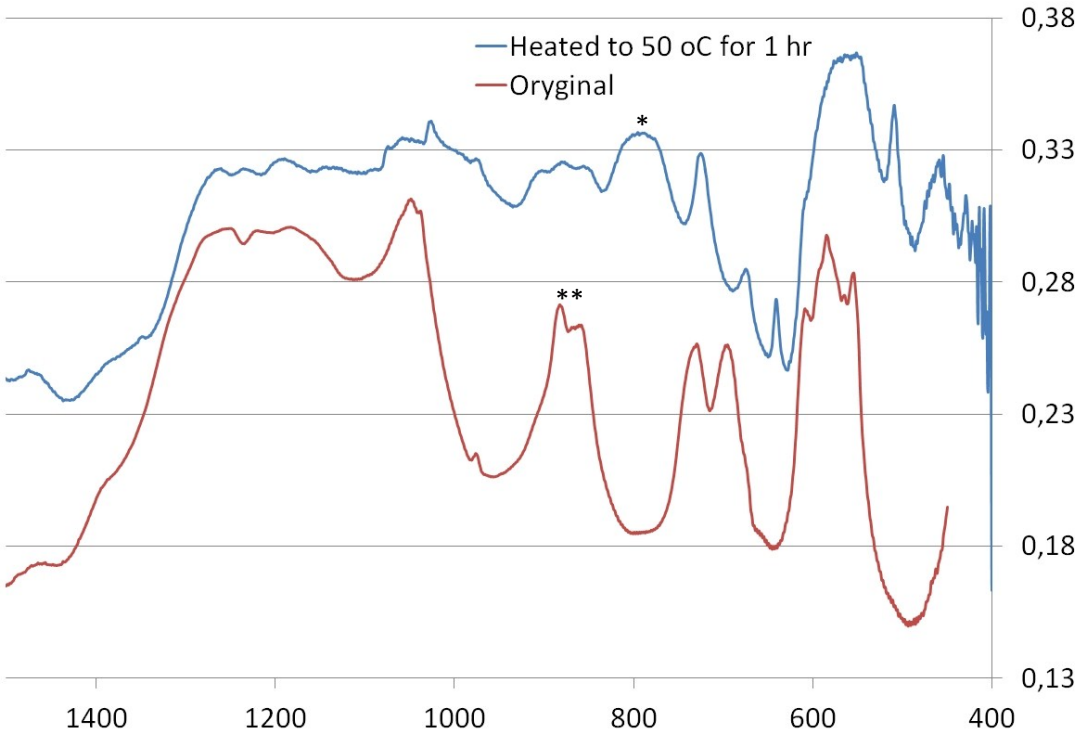

S7. Powder XRD of a sample of $Ag_2S_2O_8$ after heating to 525 °C.

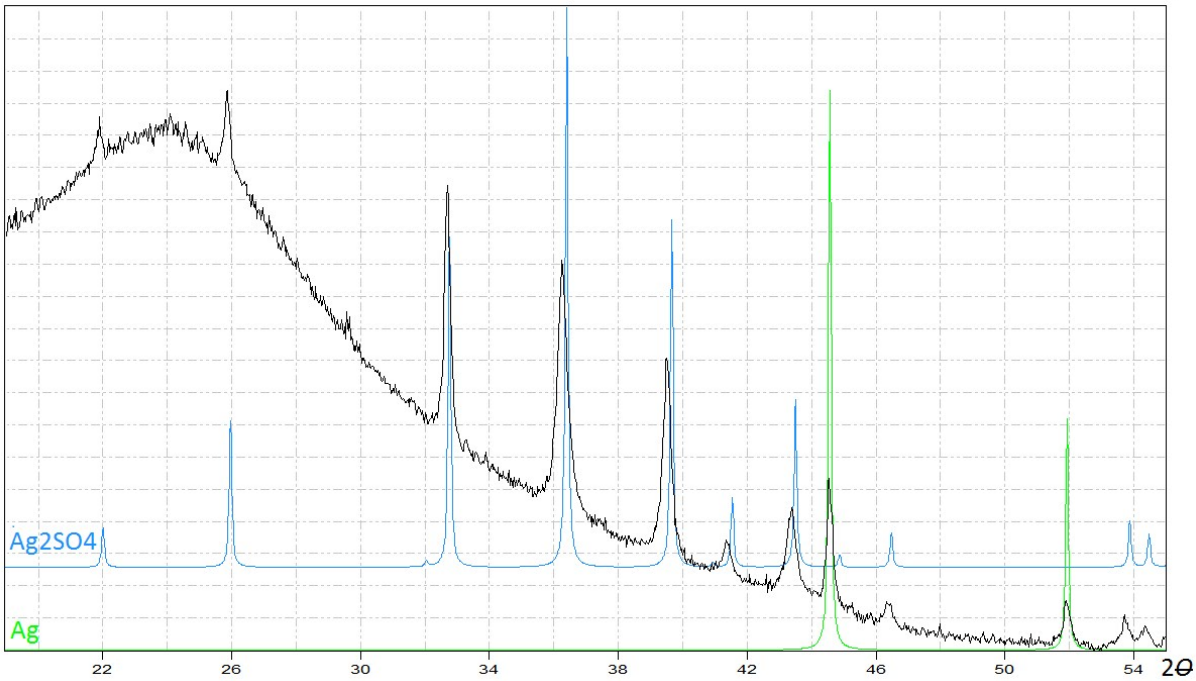

Aside from "amorphous hump", the sample consists mainly of Ag_2SO_4 (*F*ddd). Small amount of fcc silver originates from both decomposition of Ag(I) oxo-derivatives as well as crystallization of silver nanoclusters introduced during synthesis by Ag(I)[Al(O-t-C_4F_9)$_4$], or from the partial decomposition of Ag_2SO_4 at very high temperature and in Ar gas flow:

$Ag(I)_2SO_4 \rightarrow Ag(I)_2O + SO_3$ (6)

$Ag(I)_2O \rightarrow 2\ Ag(0) + ½\ O_2$ (7)

The fact that the decomposed sample contains crystalline Ag-, S- & O-species, while the evolved gas contains only S- and O-species (EGA results), additionally confirms the elemental contents (Ag, S & O) of the sample undergoing decomposition.

S8. TGA-DSC-EGA comparative analysis for $Ag(I)_2S_2O_8$ and $Ag(II)SO_4$.

Sample for coupled thermogravimetric-calorimetric-evolved gas (TGA-DSC-EGA) measurements using Netzsch thermal analyzer (for details of our experimental setup *cf.* Ref.10 to the main paper) has been preconditioned in the TGA oven at –20 °C, to obtain reliable data from 0 °C upwards. Samples mass was 14.15 mg; scan rate was 5 K/min, we used N6.0 argon as a carrier gas. Figure below shows comparison of the TGA-DSC profiles for $Ag_2S_2O_8$ (left) and the published profile for $AgSO_4$ (right) (*cf.* Ref.10 from the main paper). <u>Note! Samples mass is different in both cases.</u>

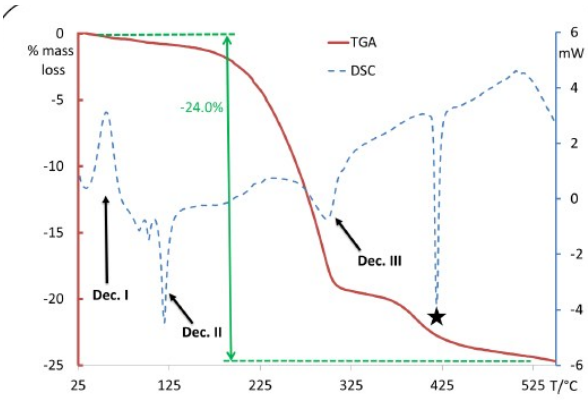

Fig 10. $Ag_2S_2O_8$ TGA/DSC measurement

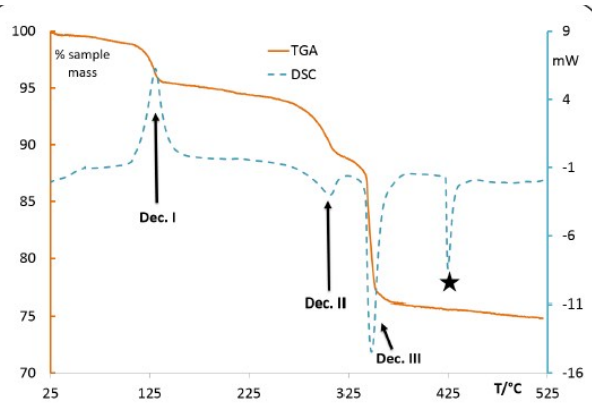

Fig 11. $AgSO_4$ TGA/DSC measurement

The TGA-DSC profiles accompanying thermal decomposition of $Ag_2S_2O_8$ and $AgSO_4$. Asterix marks the phase transition of Ag_2SO_4 final product. Note! Samples mass is different in both cases. Exothermic events – DSC maxima, endothermic – DSC minima.

Analysis of the thermal decomposition of $AgSO_4$, performed previously, is straightforward. Exothermic mass loss at 125 °C corresponds to elimination of ¼ O_2 and formation of $Ag_2S_2O_7$. The latter compound decomposes while eliminating half of SO_3 contents between 275 °C and about 350 °C. The total mass loss of ca. 24 wt. % corresponds to Ag_2SO_4 as a solid residue.
Decomposition of $Ag_2S_2O_8$ is more complex; the first exothermic event at 50 °C corresponds to Solid-solid phase transition (likely to the centrosymmetric P-1 structure), it is followed by an endothermic event with the maximum at *ca.* 120 °C; the mass loss up to 130 °C is small, some 1 wt.%, and does not constitute a clearly marked step in the TGA curve. Larger mass loss commences via several endothermal events at 150 °C and above; in contrast to $AgSO_4$ sample keeps decomposiing even at 450 °C. The total mass loss up to 520 °C is 24.0 wt.% and Ag_2SO_4 is again the final product. The behaviour of $Ag_2S_2O_8$ contrasts somewhat with that seen for related $M_2S_2O_8$ salts (M=Na, K, Rb, Cs) and it is likely due to catalytic role of Ag(I) for the accompanying reactions.

The following heat values have been determined for the particular events:

Stages of decomposition of $Ag_2S_2O_8$:
I –17.65 kj/mol
II +12.32 kJ/mol
III +13.05 kJ/mol

Stages of decomposition of $AgSO_4$:
I –53.00 kJ/mol
II +5.20 kJ/mol
III +68.95 kJ/mol

Based on these values, as well as on the fact thatthe final products of thermal decomposition of both electromers seem to be chemically identical, and neglecting the specific heat for temperature regions separating the events, one might attempt to estimate the relative stability of both electromers

(figure below). Such preliminary estimate (see figure below) suggests that $Ag_2S_2O_8$ is less stable than 2 $AgSO_4$, by 14 kJ/mol.

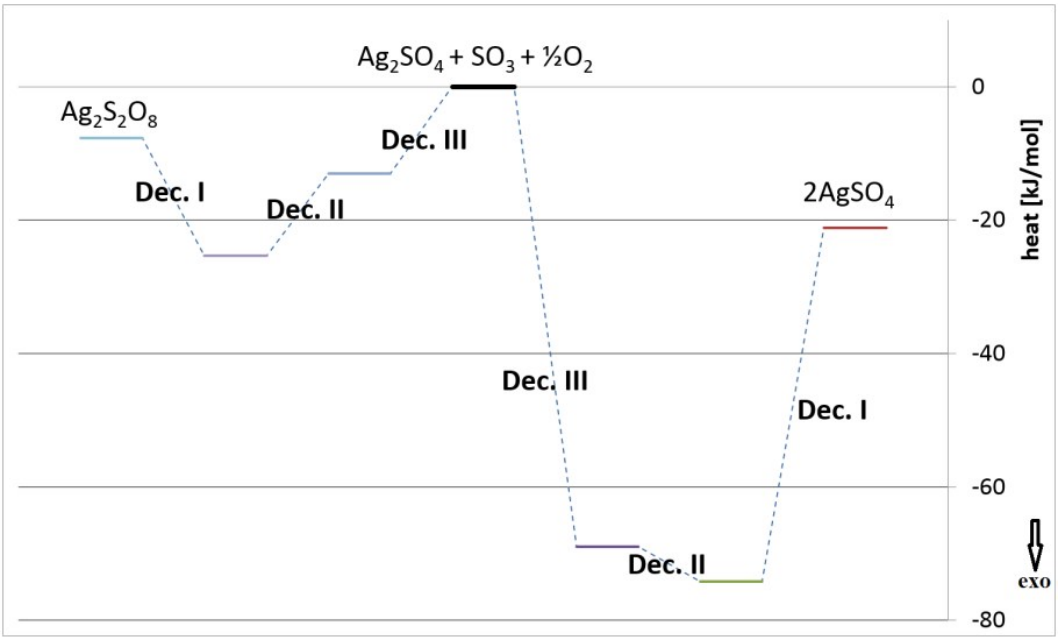

One must take this value with the large grain of salt due to (i) crude approximations mentioned above, (ii) the fact that $Ag_2S_2O_8$ is far from being 100% pure and (iii) it may partially decompose in the TGA oven while the sample is being conditioned in Ar gas, (iv) one of its impurities ($Ag_2S_2O_7$) also decomposes thermally in the temperature region studied, (v) as well as having in mind the worse than 15% precision of our DSC setup.

S9. DFT calculations for $Ag(I)_2S_2O_8$ vs. $Ag(II)SO_4$.

Theoretical calculations for $Ag_2S_2O_8$ have been difficult to do, due to artifactual polymeric nature of one of $S_2O_8^{2-}$ anions present in the fully ordered structure model which initially evolved from the powder XRD data, and the one, which assummed partial disorder of the anionic sublattice. We have attempted to resolve this problem, *e.g.* by constructing larger unit cells and shifting the $[S_2O_8]$ units with respect to each other so to obtain more chemically sound structure. Such Z=12 unit cells have always converged to a combination of Ag(II) cations and isolated SO_4^{2-} anions in our DFT calculations (PBE, cutoff 500 eV, k-mesh 0.3 $Å^{-1}$). This feature suggests that attempts to find local minimum using GGA are unsatisfactory and HSE06 should be used (regretfully, this was impossible due to large supercell size and limited computational resources). However, instability of the $Ag(I)_2S_2O_8$ formulation with respect to $Ag(II)SO_4$ one might suggest that, indeed, $Ag(II)SO_4$ is more stable one of the two. Indeed, our earlier estimates of stability using a close-to-ground state structure of $Ag(II)SO_4$, and the $K_2S_2O_8$ model of $Ag(I)_2S_2O_8$ have showed that the latter has energy higher by over 0.5 eV than the former one (INORG CHEM 2010, 49(6): 2735–2742).

The mutual transformation of electromers by different stimuli remains to be investigated; this research by necessity will be difficult due to te lack of stability and high reactivity of both electromers.

S10. Relative stability of $Ag(I)_2S_2O_8$ and $Ag(II)SO_4$ from perspective of the Maximum Hardness Principle.

It is quite interesting that $Ag_2S_2O_8$, which is a colourless compound (the lack of colour would indicate large electronic excitation energies and large concomitant reaction barriers) is quite unstable thermally. We have observed that the samples of $Ag(I)_2S_2O_8$ inevitably decompose in time even if stored at –35 ^oC; this is in contrast to the behaviour of black $Ag(II)SO_4$ which may be stored for months at room temperature and despite the lack of its thermodynamic stability as well as free-radical nature of Ag(II). Another puzzling fact is that the colourless large-band gap compound ($Ag_2S_2O_8$) seems to be less stable than the black narrow-band gap $AgSO_4$, in seeming contradiction with the *Maximum Hardness Principle* from Pearson. This is probably best explained by the fact that none of the two electromers is thermodynamically stable, and the true ground state for the Ag : S : O = 1 : 1 : 4 composition corresponds to the mixture of ½ $Ag_2S_2O_7$ and ¼ O_2. Both of these are very broad band gap insulators in the solid state.